Western States of the Combustion Institute Spring Meeting
Organized by the Western States Section of the Combustion Institute
and hosted by the California Institute of Technology
March 24-25, 2014

Size Evolution of Soot Formed in Premixed C6 Hydrocarbon Flames

Joaquin Camacho[1] and Hai Wang[1]

[1]*High-Temperature Gas Dynamics Laboratory, Mechanical Engineering Department, Stanford University, Stanford, CA 94304*

Nascent soot was examined in premixed burner stabilized stagnation (BSS) flames of *n*-hexane, 1-hexene, 2-methylpentane, cyclohexane, and benzene-oxygen-argon mixtures at a fixed carbon-to-oxygen ratio of 0.69 and maximum flame temperature of 1800 K. The evolution of the particle size distribution function (PSDF) was measured from the onset of nucleation to a later stage of growth by mobility sizing. Comparison of the PSDFs shows that qualitatively, the overall sooting processes of these flames are similar. However, the time to nucleation and the persistence of nucleation was strongly dependent on the structure of the parent fuel. For the given conditions, the fastest onset of soot nucleation was observed in flames of cyclic hydrocarbon fuels, including cyclohexane and benzene. This observation is consistent with the faster aromatics formation expected for these parent fuels. At the same time and as evidenced by the disappearance of nucleation-size particles, soot nucleation in cyclohexane and benzene flames ended sooner than in flames of non-cyclic hydrocarbon fuels. Fuel specific chemistry in cyclic hydrocarbon-fuel flames may contribute to the later depletion of soot nuclei by causing earlier particle formation and growth which subsequently allows for greater scavenging of soot precursors by the particle surface.

1. Introduction

The role of fuel structure on soot formation is investigated here in a set of canonical laminar premixed flames of *n*-hexane, 1-hexene, cyclohexane, methyl-pentane and benzene. The emphasis of the study was placed on probing the evolution of the detailed particle size distribution function (PSDF). A systematic approach was taken such that the effect of local flame temperature and carbon to oxygen ratio are isolated from the fuel structure effect. Cross comparisons of the detailed and global sooting behavior were made for the normal alkane, branched alkane, normal alkene, cycloalkane and aromatic fuels for the C_6 hydrocarbon.

In the current study, the burner stabilized stagnation (BSS) flame approach coupled with mobility sizing, described in detail elsewhere (Abid et al. 2009a, 2009b), is employed to investigate the evolution of PSDFs in nascent soot from particle nucleation to mass growth. The method is inherently intrusive to flame but the technique accounts for probe-flame perturbation explicitly by treating it, experimentally and computationally, as the downstream boundary condition of the flame. With the flow field defined, the flame temperature and species concentrations can be directly modeled using a quasi one dimensional code without imposing a measured temperature profile or correcting for artificial probe perturbation (Abid et al. 2009a). To obtain reliable radiation correction for the measured temperature and to explore the fundamental kinetic causes for the fuel structure effects, a high temperature combustion model for jet fuel surrogates is used for numerical simulations. The gas-phase kinetic model begins with small hydrocarbon oxidation chemistry and ends with 1-ring aromatic formation. Basic understanding of the competition between kinetic processes such as aromatics formation and fragmentation provides insights into soot formation (Wang and Frenklach 1997). In addition, the BSS flame configuration allows for the thermophoretic velocity of soot to be quantified within the domain thus allowing for sooting behavior to be compared in terms of residence time in the flame.

2. Experimental Methodologies

In The BSS flame approach was employed to probe nascent soot formation in the flames of C_6 hydrocarbons summarized in Table 1. One lightly sooting BSS flame was stabilized for each fuel at atmospheric pressure with maximum flame temperature of 1800K.

Table 1. Summary of the premixed BSS flame conditions. The maximum flame temperature is 1800K for each flame.

		Mole fractions[a]				Velocity[b], v_o (cm/s)
			O_2	C/O	ϕ	
n-hexane	$n\text{-}C_6H_{14}$	0.0748	0.325	0.69	2.19	4.57
2-methylpentane	$i\text{-}C_6H_{14}$	0.0748	0.325	0.69	2.19	4.57
1-hexene	$n\text{-}C_6H_{12}$	0.0748	0.325	0.69	2.07	3.85
Cyclohexane	$c\text{-}C_6H_{12}$	0.0748	0.325	0.69	2.07	4.87
Benzene	C_6H_6	0.0748	0.325	0.69	1.72	3.41

[a] The balance gas is argon (X_{Ar} = 0.6) [b] STP cold gas velocity

Furthermore, the total *C/O* ratio of the flames was held fixed at *C/O* = 0.69. The adiabatic flame temperature for benzene is much greater than the other flames because the equivalence ratio is closer to unity. Thus the cold gas velocity of the benzene flame is lower than the flow rate of the other fuels to match the 1800 K flame temperature constraint. The gas temperature profiles were measured with a Y_2O_3/BeO coated type-S thermocouple with radiation correction using a procedure discussed earlier (Abid et al. 2008). The bead diameter was approximately 0.3 μm after coating.

The flat flame burner is 5 cm in diameter and is uncooled because of potential condensation of the fuel in the porous material. Without water cooling, however, the pores tend to close in its center over time, thus modifying the local unburned gas velocity. For this reason, fresh porous material was always used to keep the flame roughly one dimensional. A sheath of nitrogen shields the flame to prevent radial entrainment and diffusion of oxygen from ambient air. The C_6 hydrocarbon fuels, supplied by Sigma-Aldridge (ACS Reagent grade, 99% purity), were injected into the fuel line and vaporized in a manner similar to a previous study of dodecane BSS flames (Abid et al. 2009b). The mass flow rates of oxygen, argon and nitrogen were measured by critical orifices and the flow of argon driving the fuel nebulizer was calibrated by a bubble displacement.

Particle size distributions were determined with a TSI 3080 SMPS (Electrostatic Classifier 3085 and UCPC 3080, AIM Software V.8.1) using a sample dilution technique developed earlier and improved over time (Abid et al. 2008, Abid, et al. 2009c, Zhao et al. 2003a, Zhao et al. 2003b and Zhao et al. 2007). The sample gas entered the probe through an orifice and was immediately diluted with a cold nitrogen flow to prevent particle losses. The dilution range and calibration has been used before and care was taken to avoid diffusion losses, condensation of higher-molecular weight hydrocarbons, and probe-induced particle-particle coagulation during dilution (Abid et al. 2009). Limitations of the Cunningham slip correction cause particles below 10 nm to be overestimated by mobility measurements and thus a nanoparticle transport theory was used for small particles to obtain more accurate particles sizes (Li et al. 2003a, Li et al. 2003b and Singh et al. 2007).

The experimentally measured temperature profiles are radiation corrected by using transport and flow properties that are calculated by a modified version of OPPDIF (Abid et al. 2009a, Kee et al. 1989). The ratio of the burner-to-probe separation to the burner diameter is much less than unity so the quasi one-dimensional assumption applies. The flame chemistry for the C_6 hydrocarbons was calculated with a reduced JetSurF mechanism (Sirjean et al. 2010) to be introduced below. By energy conservation, the modified OPPDIF code allows for the calculation of the temperature and species profile without the need for a measured temperature profile as an input. The radiation corrected temperature profiles are compared to the calculated OPPDIF profile to test the validity of the experimental and numerical procedures. The temperature closest to the burner surface that can be measured is equal to one half of the thermocouple bead diameter (0.15 mm). The inlet temperature was extrapolated from the measured temperature profile immediately adjacent to the burner surface. The temperature variation is roughly linear with respect to the distance, as one would expect because in that region the dominant heat transfer mechanism is heat conduction. The probe temperature was measured with a type K thermocouple embedded on the stagnation surface.

The flame perturbation due to the sampling probe is included in the modified OPPDIF code by introducing a stagnation surface at $x = H_p$ in the form of a zero velocity boundary condition (Abid et al. 2009). The flow stagnation causes the fluid velocity and hence the convective time for soot nucleation and growth to increase dramatically. For soot particles, the finite residence time is determined by considering the thermophoretic velocity which is driven by the significant temperature gradient, dT/dx, at the stagnation plate. In this study, the thermophoretic velocity of the particle within the flame will be calculated in the hard sphere and diffuse scattering limit (Li & Wang 2004):

$$V_T = \frac{\lambda\ \partial \mathrm{T}/\partial \mathrm{x}}{5\left(1+\frac{\pi\varphi}{8}\right)NkT} \qquad (1)$$

where λ is the thermal conductivity of the gas calculated from the flame gas. $\varphi = 0.9$ is the momentum accommodation factor, N is the gas number concentration, k is the Boltzmann constant. The thermophoretic velocity was calculated numerically and added to the axial convective velocity. The residence time of the soot particles is defined as the time interval for the particle (or precursors) to traverse from the calculated location of the peak flame temperature to the location of the stagnation probe, H_p.

3. Results and Discussion

Local temperature is the dominant parameter which governs the soot chemistry. A comparison between the measured/radiation corrected and the simulated temperature profile is shown in Fig. 1 for *n*-hexane at a series of burner-to-stagnation surface separation distances. The degree to which the stagnation probe causes heat loss is shown. The boundary condition gives rise to a different flame at each sampling distance. However, the inlet and probe are the only temperatures required to model the flame for the given flow rate and sampling distance. The agreement between the radiation corrected measurements and the simulated temperatures is within the thermocouple position uncertainty (± 0.3 mm) and the temperature measurement uncertainty (± 70 K around the peak temperature region). The temperature profiles for the other fuels studied are similar.

The temperature profiles measured and simulated for all the fuels studied is shown in Fig. 2 for H_p = 1.2 cm. Each fuel has a different inlet flow rate thus each residence time and local temperature is slightly different for the given boundary conditions. For example, the calculated benzene flame temperature peaks slightly sooner but the post-flame region is colder due to the lower cold gas velocity. The model solves the energy equation without the measured temperature profiles as the input. Thus, agreement between radiation corrected measurements and the simulation addresses uncertainty within the calculated local heat release and loss rates (Abid et al. 2009). Uncertainty within the simulated local flame temperature along with the resulting Arrhenius reaction kinetics and species transport can be defined with this information. In addition, the agreement between the measurement and computation confirms that the flame conditions are comparable and that sooting behavior can be observed under similar local temperature.

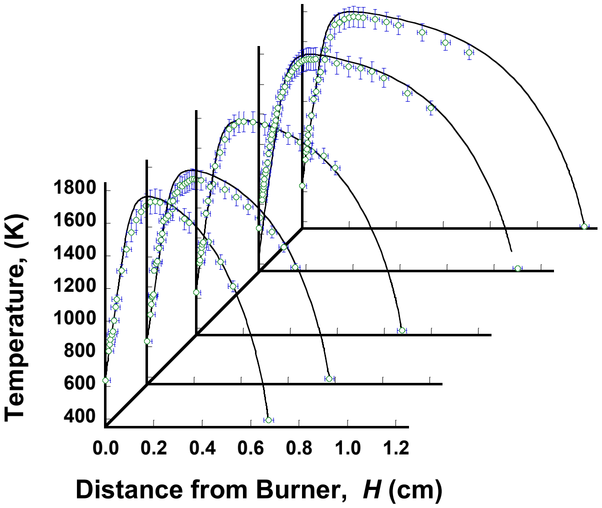

Figure 1. Measured (symbols) and simulated (lines) temperature profiles for the n-hexane flames at the given sampling locations, H_p. The vertical error bars represent the uncertainty in thermocouple radiation corrections as described in the text.

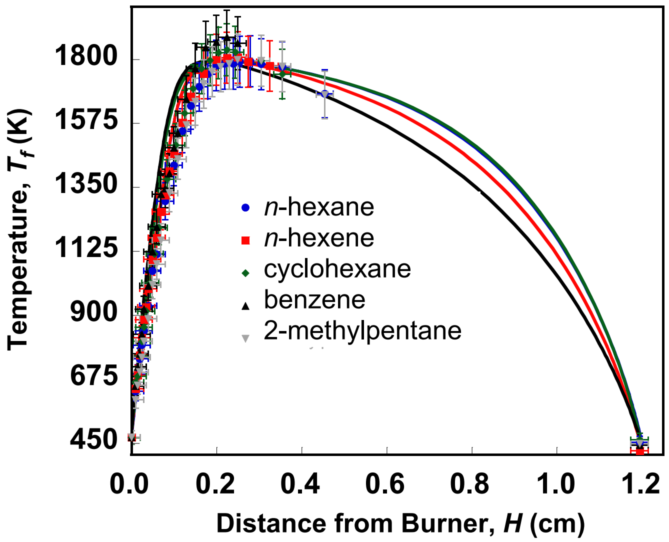

Figure 2. Measured (symbols) and simulated (lines) temperature for the C_6 hydrocarbon flames compared with H_p = 1.2 cm. The thermocouple radiation correction for methylpentane was estimated from the flame composition and transport properties of n-hexane.

Detailed sooting behavior is examined in terms of particle size for the sooting flames of C_6 hydrocarbons. In this work, the primary method to determine the particle size distribution is to measure the mobility of soot via the SMPS system described earlier. Recent Helium-Ion Microscopy (HIM) and Atomic Force Microscopy (AFM) studies have led to observations that nascent soot particles begin to deviate from the spherical primary particle shape much small in particle size than expected (Schenk et al. 2013). This observation has immediate implications to the current work. Because in the large Knudsen number limit the mobility is a measure of the particle surface area (Li & Wang 2004), we chose to report the current measurements in the form of surface area distribution rather than the particle diameter distribution.

The evolution of the PSDF from the onset of nucleation size particles to later growth stages is measured for the C_6 fuels. As examples, Fig. 3 shows the PSDFs for a series of sampling locations of the 1-hexene and cyclohexane flames. In the figure, the smallest surface area corresponds to a spherical equivalent diameter of 2.4 nm. The evolution of the PSDFs is qualitatively similar among all flames studied here. The onset of soot nucleation is followed by the formation of a bimodal PSDF indicating persistent nucleation (Zhao et al. 2003). In addition, the trough between the nucleation and growth particle sizes is roughly 10 nm in all flames, which suggest the monomer chemistry to be similar (Singh et al. 2006).

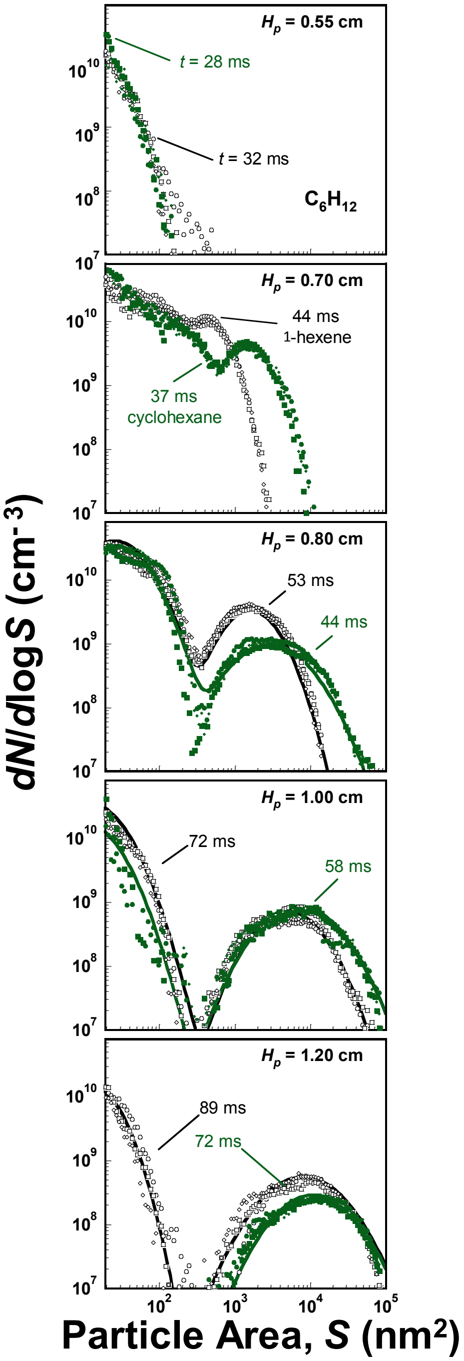

Figure 3. Measured PSDFs for 1-hexene (open symbols) and cyclohexane (filled symbols) flames expressed as a function of the particle surface area. Bimodal distributions (solid lines) are fit to highlight nucleation size particles that persist late in the flame.

Quantitatively, notable differences are observed for the different fuels. It can be seen from Fig 3. that although nucleation occurs around H_p = 0.55 cm for both 1-hexene and cyclohexane flames as evidenced by the burst of particles entering into the detectable size window, The size distribution of soot develops later in the 1-hexene, slower than that in the cyclohexane flame. Here, we note that the difference in the residence time at each position of the two flames is the result of different cold gas velocities used so as to achieve the same flame temperature.

Another difference between nascent soot of the C_6H_{12} isomers is the intensity of the nucleation mode within the PSDF. Nucleation persists late for both flames but the nucleation size particles become undetectable for $H_p = 1.2$ cm in the cyclohexane flame. Here, we note that for the fuels considered above, the most significant fuel structure effect is in cyclohexane flames where there is a relatively early start to soot nucleation followed by a relatively early end to nucleation.

Soot volume fraction, F_v, was determined for each flame by integrating the PSDF over all particle sizes measured ($2.4 < D_p < 166.5$ nm), assuming that the particles are spherical. The volume fraction data are shown in Fig. 4 as a function of H_p, and the particle residence time. It is clear from the top two panels that with the exception of 1-hexene, the volume fractions measured for all fuels collapse on the same curve for large H_p values, despite the small difference seen in the time to onset of nucleation. This observation follows the well-established notion that the rate soot production in the premixed flame is governed predominantly by the maximum flame temperature and C/O ratio rather than the structure of the fuel. However, care must be taken here when interpreting the data. The flames compared here have different hydrogen contents and the post flame temperatures. It is possible that any chemistry effects due to the different fuel structure is canceled out with one or more flame properties that could not be kept constant. Hence, the similarity in the variation of the soot volume fraction as a function of the residence time observed here may be fortuitous. Also for comparison, soot volume fraction profiles are also compared on the basis of equal equivalence ratio ($\phi = 2.07$) as shown in the bottom panel of Fig. 4. The volume fraction was found to increase with the C/O ratio of the flame as expected.

The impact of the parent fuel structure can be examined more closely when both the equivalence ratio and *C/O* ratio are identical. This basis of comparison is shown in Fig. 5 for the cyclohexane, 1-hexane and ethylene flames in terms of the soot volume fraction and number density. The ethylene flame is similar to the BSS flame reported previously (Abid et al. 2009) with the flame temperature slightly decreased to match the current study. The impact of the parent fuel structure becomes quite apparent here, as seen by the different final soot volume fraction, number density and nucleation time. The hierarchy of the soot volume fraction resembles the relative trend observed in non-premixed flames where aromatic structures and higher carbon number increase soot production. The particle number density in the cyclohexane flame shown in Fig. 5 is relatively small because nucleation size particles stop forming as discussed above.

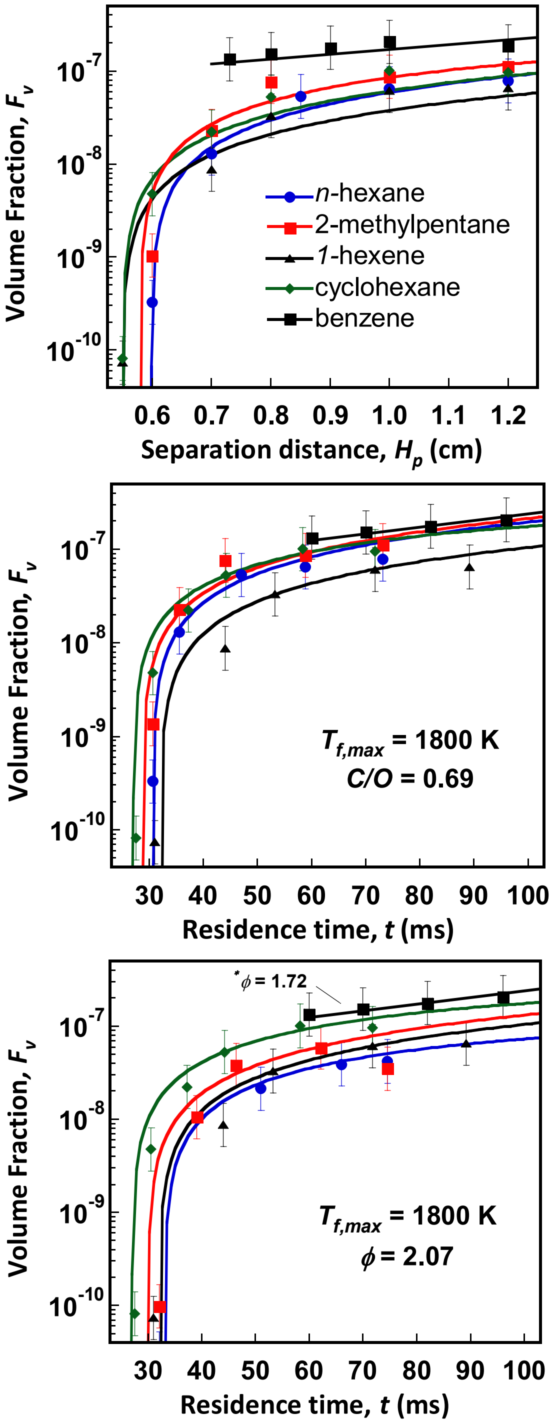

Figure 4. Volume fraction of nascent soot with $D_p > 2.4$ nm (symbols) measured for all the fuels studied as function of sampling distance (top panel) and particle residence time (bottom panel). For the $\phi = 2.07$

comparison (bottom panel), the benzene flame shown has $\phi = 1.72$ because the production of soot for $\phi = 2.07$ increases to beyond the measurable limit. Lines are drawn to guide the eye.

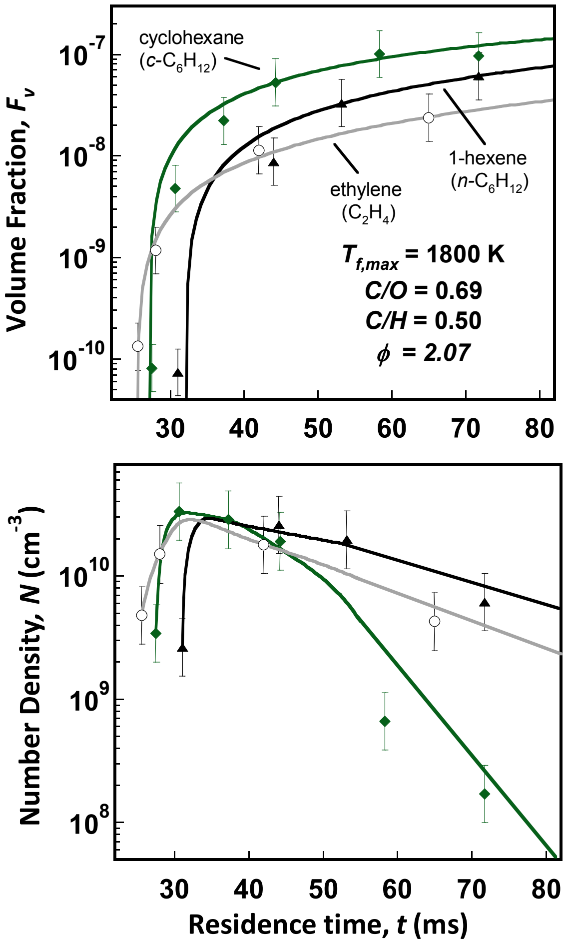

Figure 5. Volume fraction (top panel) and number density with $D_p > 2.4$ nm (bottom panel) for the cyclohexane, 1-hexene, and ethylene flames (C/O = 0.69) studied. Lines are drawn to guide the eye.

4. Conclusions

Soot formation was studied from the onset of nucleation to later growth stages in premixed burner stabilized stagnation (BSS) flames of five C_6 hydrocarbons. The overall sooting process was found to be comparable among the fuels under similar flame condition. The nucleation time and the persistence of nucleation with time were found to be dependent on the structure of the parent fuel. The fastest onset of soot nucleation was observed in cyclohexane and benzene flames and this may be due to more significant aromatics formation earlier in the flame. In addition, the evolution of the PSDF showed that nucleation ends sooner in cylclohexane and benzene flames and this behavior is related to the scavenging of small particles by the surface of much larger particles.

5. Acknowledgements

This material is based upon work supported as part of the CEFRC, an Energy Frontier Research Center funded by the U.S. Department of Energy, Office of Science, Office of Basic Energy Sciences under Award Number DE-SC0001198.

6. References

Abid, A.D., Tolmachoff, E.D., Phares, D. J., Wang, H., Liu, Y., Laskin, A. (2009) *Proc. Combust. Inst.* 32, 681-688.
Abid, A.D., Camacho, J, Sheen, D.A. and Wang, H. (2009) *Combust. Flame* 156, 1862-1870.
Abid, A.D., Camacho, J, Sheen, D.A. and Wang, H. (2009) *Energy Fuels* 23, 4286-4294.
Wang, H., Frenklach, M. (1997) *Combust. Flame* 110, 173-221.
Abid, A.D., Heinz, N., Tolmachoff, E.D., Phares, D.J., Campbell, C., Wang, H. (2008) *Combust. Flame* 154, 775-788.
Sirjean, B., Dames, E., Sheen, D. A., You, X., Sung, C. J., Holley, A. T., Egolfopoulos, F. N., Wang, H., Vasu, S. S., Davidson, D. F., Hanson, R. K., Pitsch, H., Bowman, C. T., Kelley, A., Law, C. K., Tsang, W., Cernansky, N. P., Miller, D., Violi, A., Lindstedt, R.P. (2010) A high-temperature chemical kinetic model of n-alkane (up to n-dodecane), cyclohexane, and methyl-, ethyl-, n-propyl and n-butyl-cyclohexane oxidation at high temperatures, JetSurF version 2.0, September 19, 2010 (http://melchior.usc.edu/JetSurF/JetSurF2.0).
Li, Z. G., Wang, H. (2003) *Phys. Rev. E* 68, article 061206.
Li, Z. G., Wang, H. (2004) *Phys. Rev. E* 70, article 021205
Schenk, M., Lieb, S., Vieker, H., Beyer, A., Golzhauser, A., Wang, H., Kohse-Hoinghause, K. (2013) *Chem. Phys. Chem.* 14, 3248 – 3254.
Singh, J., Patterson, R. I. A., Kraft, M., Wang, H. (2006)_*Combust. Flame* 145, 117-127.
Kee, R.J., Miller, J. A., Evans, G. H., Dixon-Lewis, G. (1989)_ *Symp. (Int.) Combust*. 22, 1479-1494.
Wang, H. (2001) Proc. Combust. Inst. 33, 41-67.
Zhao, B., Yang, Z. W., Wang, J. J., Johnston, M. V., Wang, H. (2003) *Aerosol Sci. Tech.* 37, 611-620.
Zhao, B., Yang, Z. W., Johnston, M. V., Wang, H., Wexler, A. S., Balthasar, M., Kraft, M. (2003) *Combust. Flame* 133, 173-188.
Zhao, B., Uchikawa, K., Wang, H. (2007) *Proc. Combust. Inst.* 31, 851-860.